High Energy Astrophysics and Cosmology in the era of all-sky surveys

Yerevan, June 15-19 2026

SCIENTIFIC ORGANIZING COMMITTEE

Sudip Bhattacharyya (TIFR, Mumbai)
Niel Brandt (Penn State)
Andrei Bykov (Ioffe Inst., St.Pete
Massimo Della Valle (INAF-Napo
Elena Gallo (Michigan Univ)
Marat Gilfanov (Co-chair, MPA)
Paolo Giommi (INAF-MILAN)
Zoltan Haiman (ISTA)
Luis Ho (KIAA Peking Univ)
Andrey Kravtsov (Chicago Univ.)
Di Li (NAO, Shanghai)
Alexander Lutovinov (IKI, Moscow)
Felix Mirabel (Univ. Buenos Aires, DAP-CEA Saclay)
Razmik Mirzoyan (MPIfP, Garching)
Maria Petropoulou (Athens Univ)
Vahe Petrosyan (Stanford)
Tsvi Piran (Hebrew Univ, Jerusalem)
Konstantin Postnov (Sternberg Inst, Moscow),
Remo Ruffini (ICRANet)
Narek Sahakyan (Co-chair, ICRANet Armenia)
Alexandra Veledina (Turku Univ)
Alexey Vikhlinin (CfA)
Shuang-Nan Zhang (IHEP, Beijing)

Selected Results from Ground-based Gamma-Ray Astrophysics & Near-Future Prospects

Razmik Mirzoyan

Max-Planck-Institute for Physics, Munich, Germany

National Academy of Sciences of Republic Armenia, Yerevan, Armenia

LOCAL ORGANIZING COMMITTEE

Damien Bégué (Co-chair, BIU)
Mher Khachatryan (ICRANet Armenia)
Ivetta Hakobyan (ICRANet Armenia)
Vika Markosyan (ICRANet Armenia)
Davit Israyelyan (ICRANet Armenia)
Narek Sahakyan (Co-chair, ICRANet Armenia)
Artyom Khachatryan (ICRANet Armenia)
Vazgen Vardanyan (ICRANet Armenia)

https://indico.global/event/16224/
Contact: heacoss2026@gmail.com

Foto: DALL-E 3

Important developments in ground-based γ-ray astronomy

1952-1953 – discovery of Cherenkov pulses in atmosphere with a 0,25m ø mirror and a 2‘‘ PMT

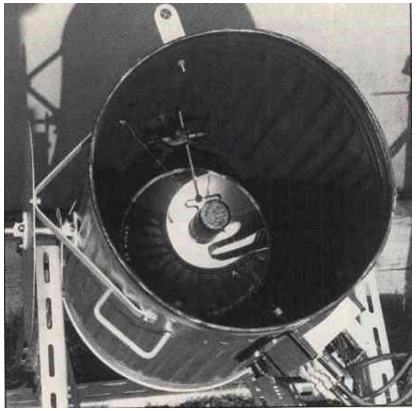

1959-1964 - Chudakovs experiment in Crimea
12 x 1,55m ø parabolic mirrors (total ~21 m²)

1968-2003 - 10m ø Whipple telescope AZ, USA

Atmospheric Cherenkov Telescopes in the Early 1960‘s

10 m Whipple ACT for ground-based VHE astrophysics

Whipple Telescope 1968

T. Weekes et al., ApJ 342 (1989) 379

"Observation of TeV Gamma Rays from the Crab Nebula using the Atmospheric Cerenkov Imaging Technique"

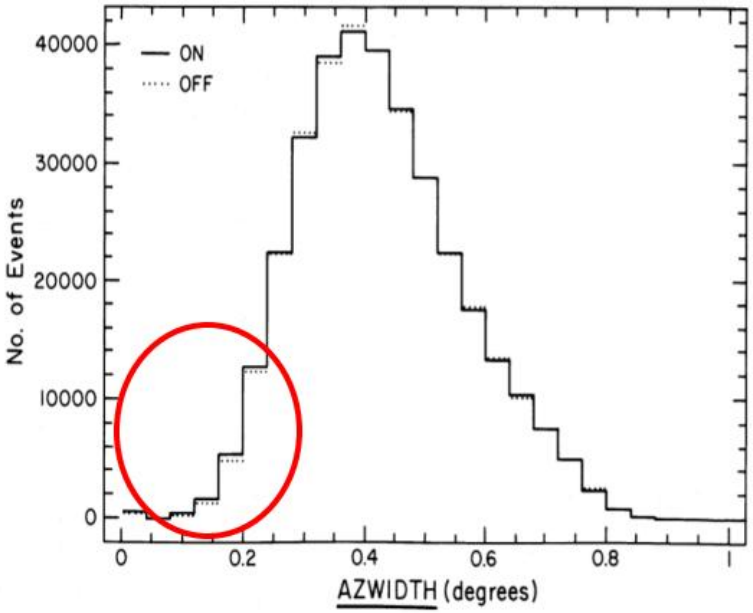

The 1st IACT (of 5 planned) we´ve built in 1989 near Yerevan

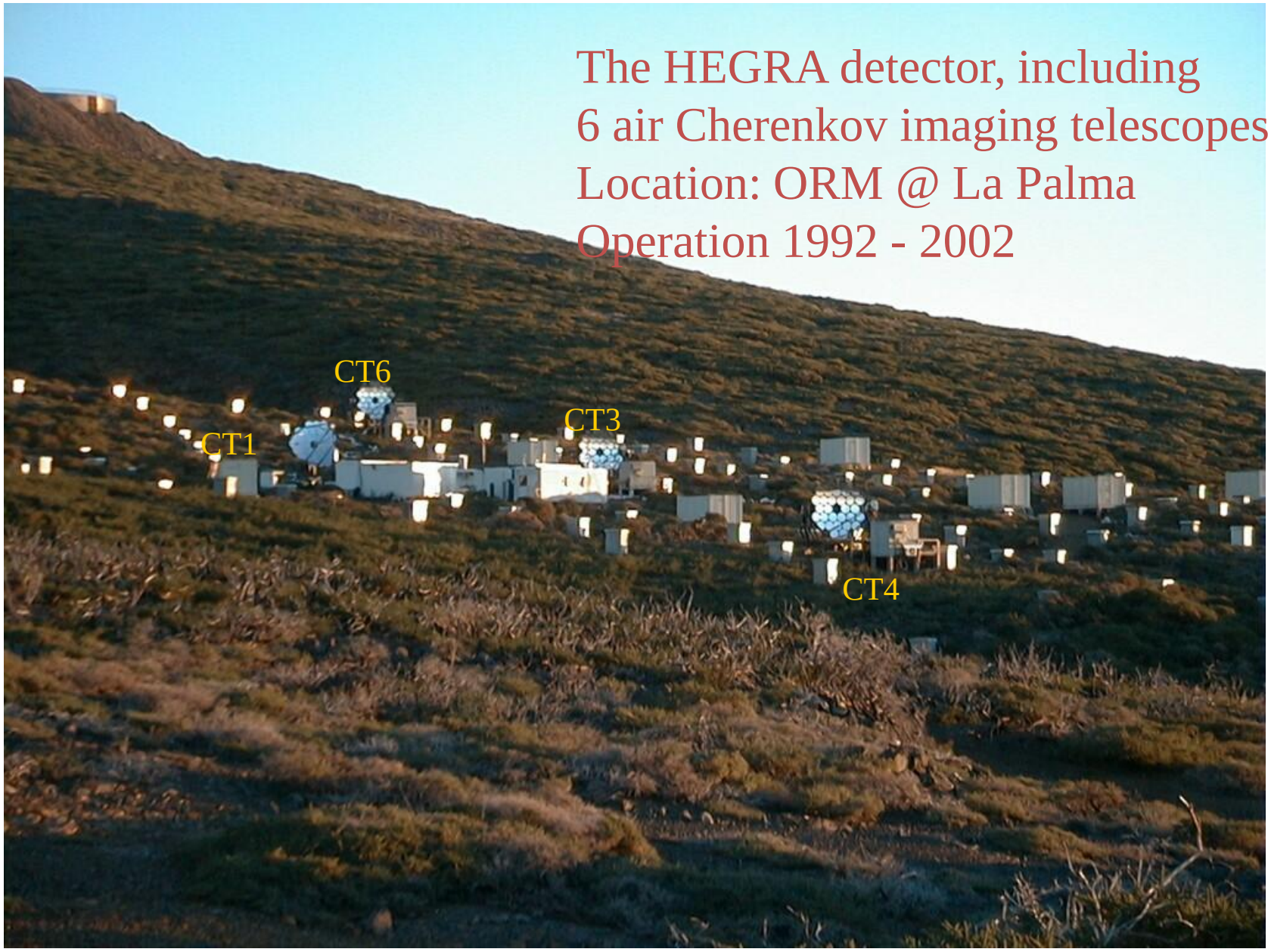
The HEGRA detector, including
6 air Cherenkov imaging telescopes
Location: ORM @ La Palma
Operation 1992 - 2002
CT6
CT1
CT3
CT4

CTA IACT designs, some more successful than the others (the majority did not survive)

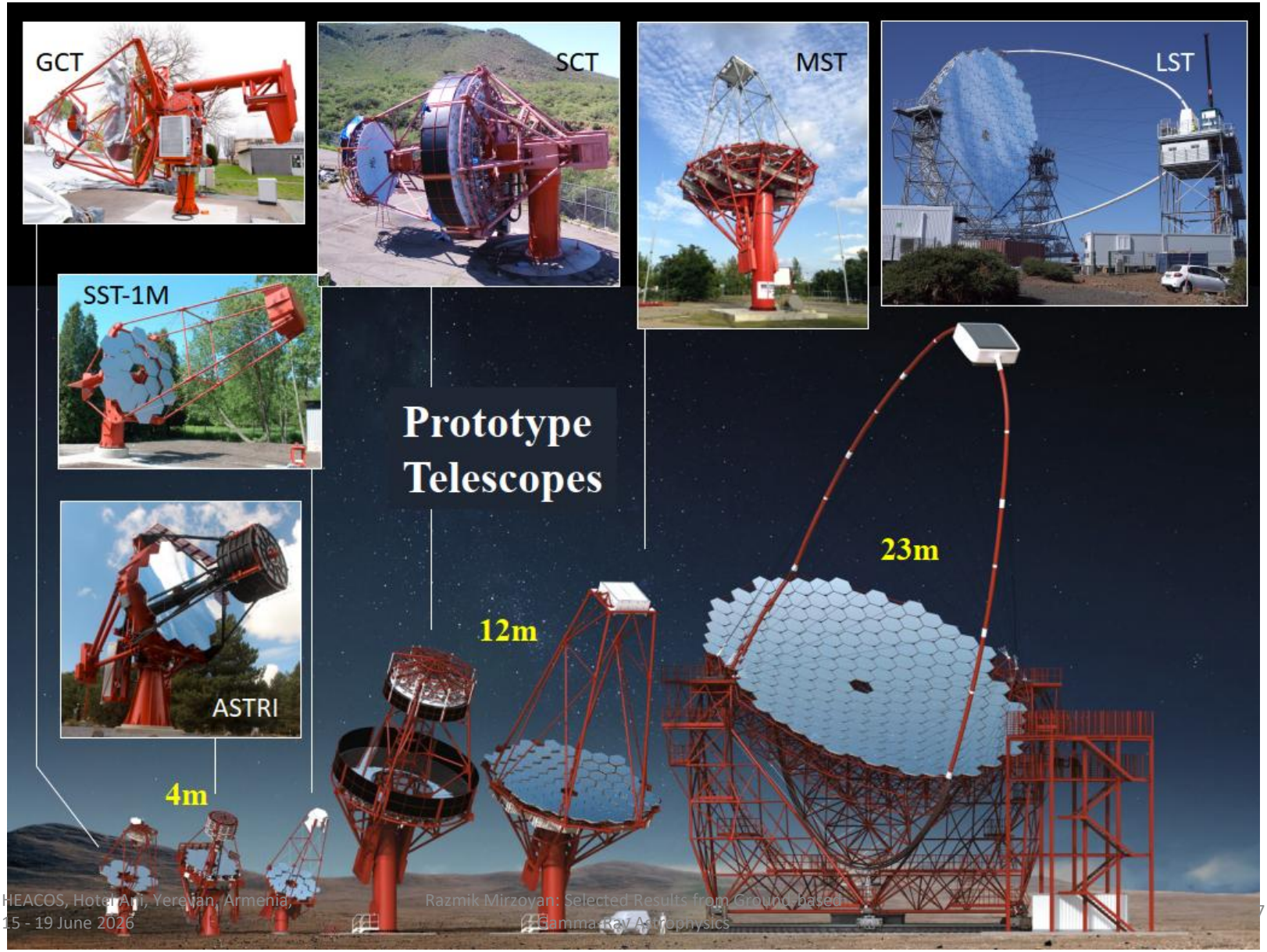

VERITAS, H.E.S.S., MAGIC and since 2019 also the 1st 23m Ø CTA/LST: at the frontier of VHE γ-astro-physics

MAGIC Telescope

- Sensitivity: 0.6% Crab in 50h obs.
- Located in LaPalma, Canary islands, Spain, 2200m a.s.l.
- Two f/1, 17 m telescopes at 85m
- ns-fast opto-electronic design
- 20s repositioning time to transients
- FoV: 3.5 degrees
- Energy range:
  Standard trigger: 50 GeV - 100 TeV
  SUM-Trigger: 20 GeV – 100 TeV
- Angular resolution
  0.084° > 0.2 TeV; 0.072° > 1 TeV
- Energy Resolution
  ~ 20% from 0.1 to 10 TeV

Milestones in VHE γ astro-physics

- 2nd generation imaging telescopes, lead by the pioneering 10m Ø Whipple telescope, made the breakthrough, in the first time allowing to measure reliably γ sources at E ≥ 700 GeV
- 2nd generation telescope arrays, put in proximity and set into coincidence (later on dubbed as „Stereo“), led by HEGRA, allowed increasing the sensitivity and precision of measurements
- 3rd generation telescope MAGIC was 1st to lower the operational energy range of an IACT by one order of magnitude, down to 25 GeV (discovery of γ pulses from Crab pulsar at E ≥ 25 GeV, SCIENCE,2008)

Since 2019 the 23m ø LST1 is taking data and publishing papers

HAWC

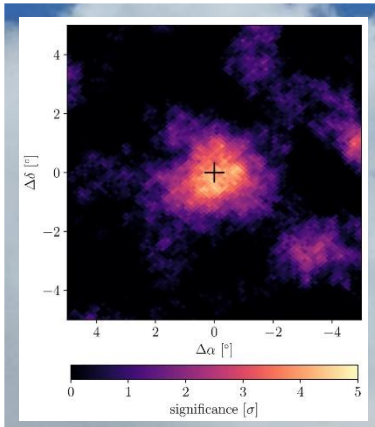

Gamma-Ray signal from the Sun @ few TeV

High Altitude Water Cherenkov (HAWC) detector

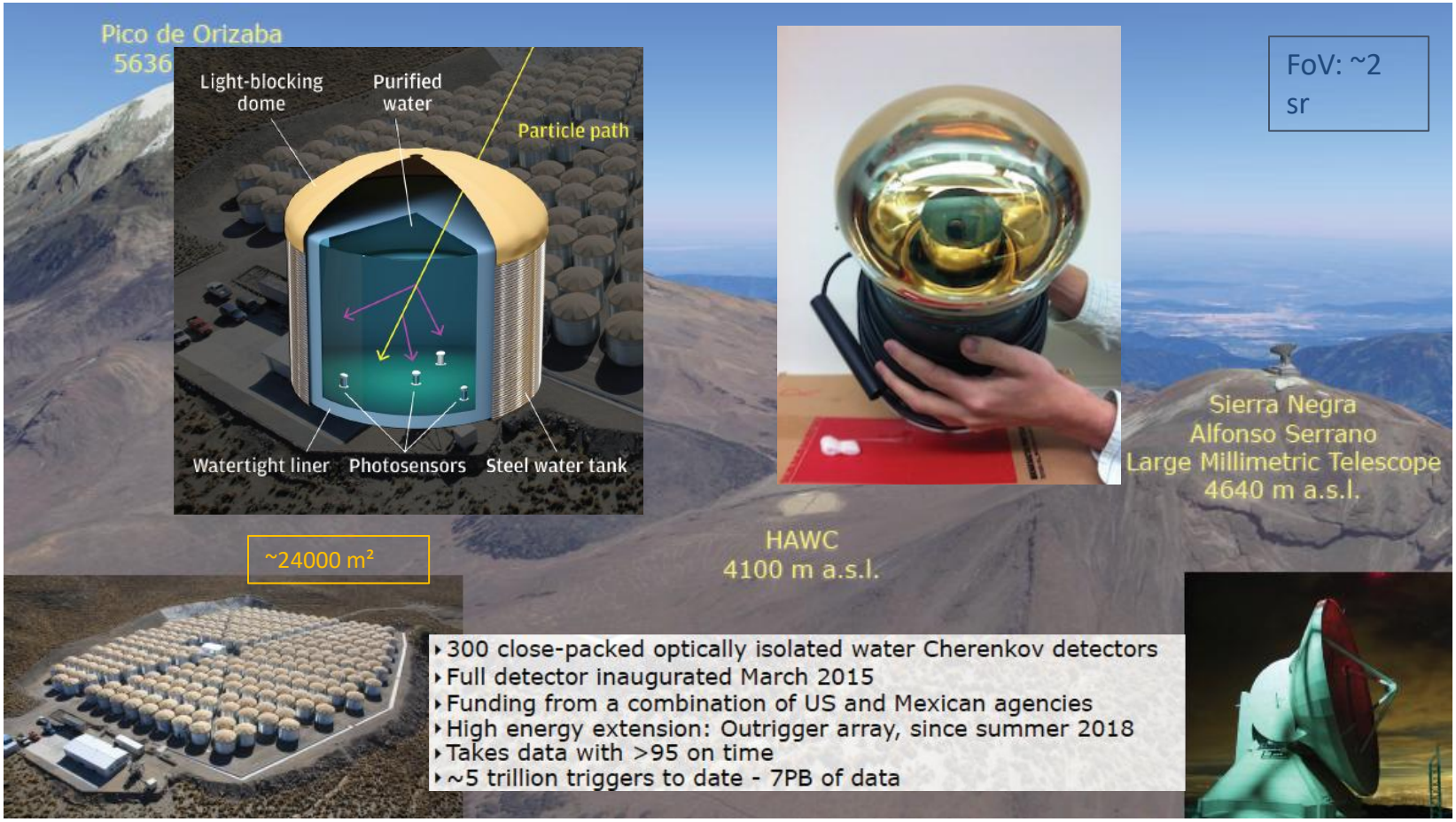

Hybrid Detection of EASs by LHAASO

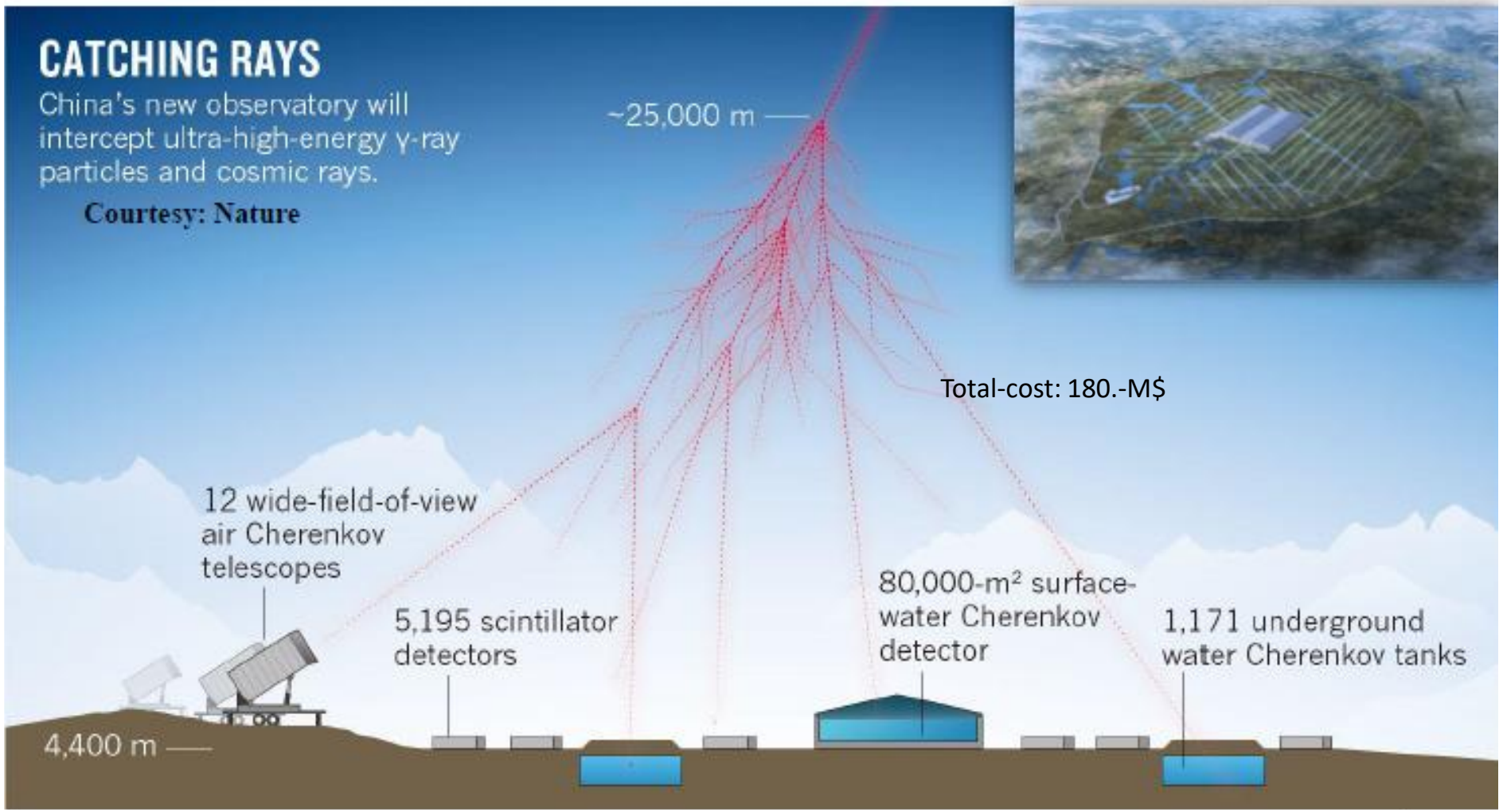

LHAASO and upgrade plans with LACT

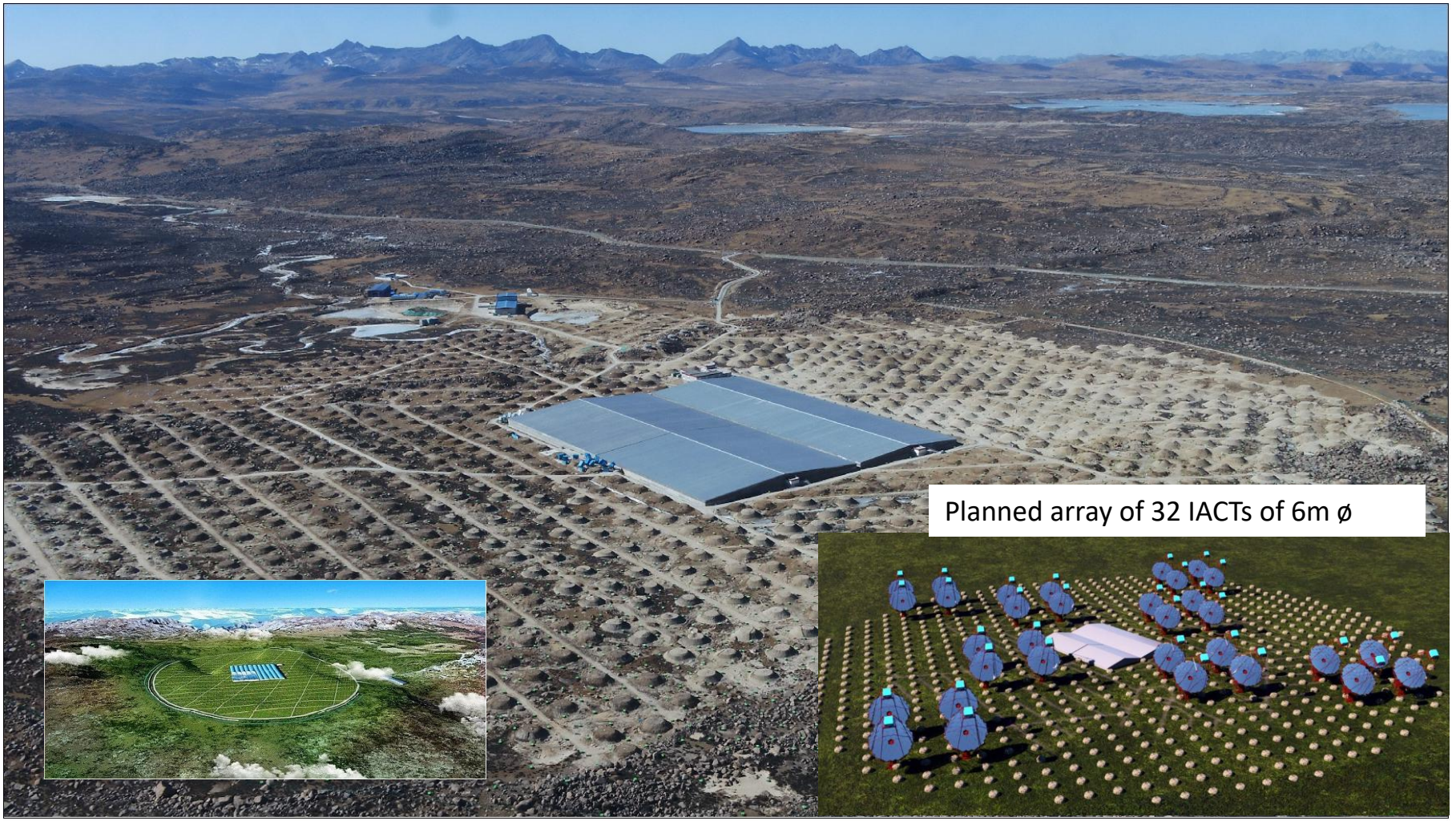

M87

- Distance: 16.8 Mpc
- Weakly accreting supermassive black hole (SMBH) of ~6.5 x 10^9 $M_\odot$
- Relativistic collimated jet
- Viewing angle 17° No strong Doppler boosting

- Detected in all energy bands
- TeV flux variable,
- Inconclusive MWL bahvior

- **Aim: study the origin of gamma-ray emission**
  - Need MWL observations to distinguish between emission models close to SMBH and further away in the jet
  - Variability and possible MWL correlation

NASA, ESA and the Hubble Heritage Team (STScI/AURA); Acknowledgment: P. Cote (Herzberg Institute of Astrophysics) and E. Baltz (Stanford University)

M87 – 2017 campaign

- Most extensive quasi-simultaneous data set
- Resolved structures from radio to X-rays
- Spatial resolution of instruments ranging 20 μas – 2°
- M87 in relatively low state in all wavebands
- First observational campaign published in ApJL, 911 L11, April 2021
- Considered as the reference quiescent state data set

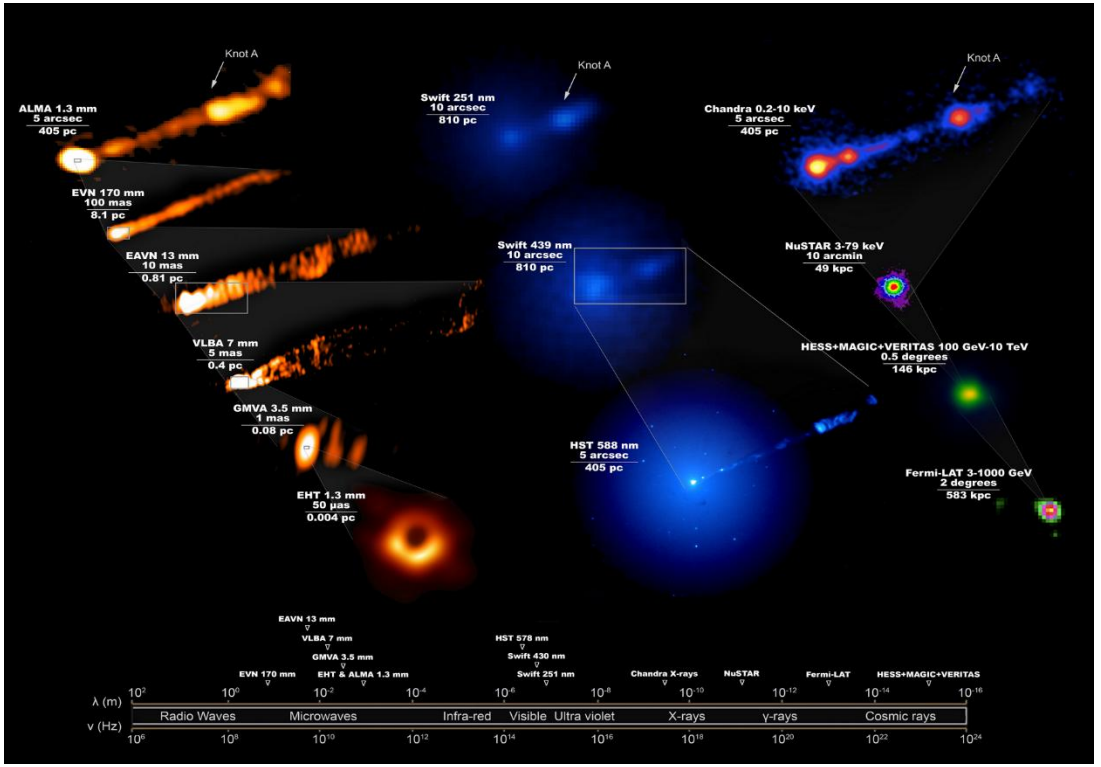

Press release image 2021; image Credit: The EHT MWL Science WG; EHT; ALMA (ESO/NAOJ/NRAO); EVN; EAVN; VLBA (NRAO); GMVA; HST, Neil Gehrels Swift Obs.; Chandra; Nucl. Spectros. Tel. Array; Fermi-LAT; H.E.S.S.; MAGIC; VERITAS; NASA, ESA. Composition by J.C. Algaba.

M87
2018 VHE gamma-ray flare

- During the 2018 MWL campaign H.E.S.S., MAGIC and VERITAS detected a short VHE (>100 GeV) gamma-ray flare
- First observed flare since 2010 (>3 σ over constant flux)
- Short time scales: from observed variability time scale $R_{VHE,\,flare} \simeq 2\ R_{EHT}$ for Doppler factor = 1
- Hint for spectral hardening during flux increase
- Published in A&A, 692:A140, Dec. 2024

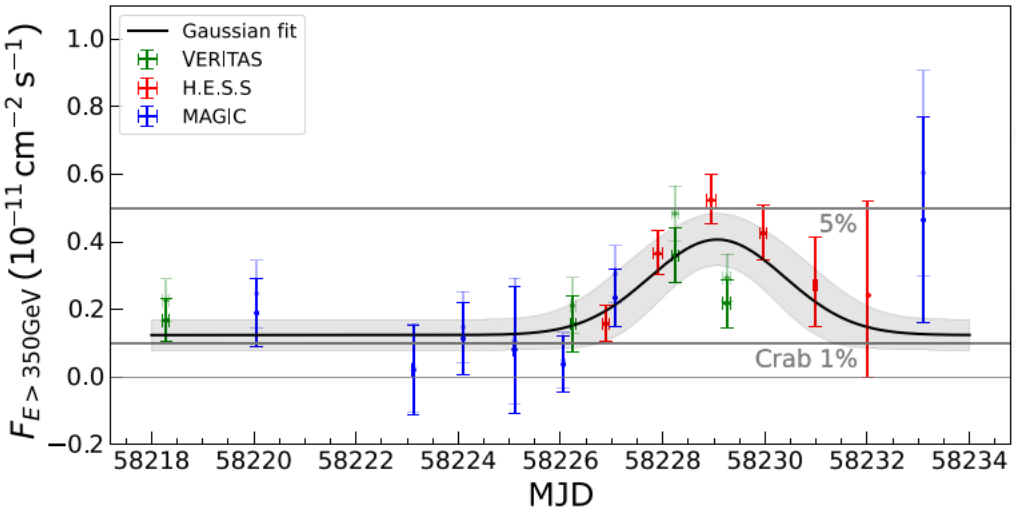

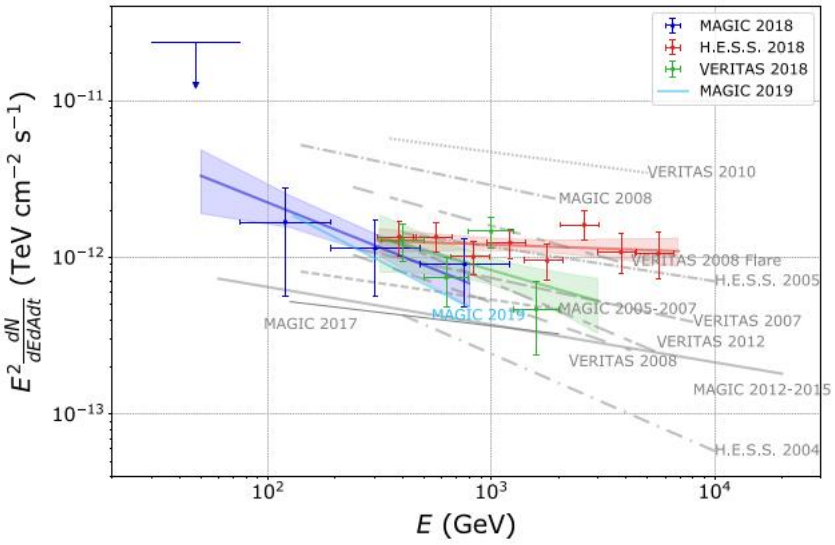

M87

2018 flare SED modeling

- To model the flare
  - Freeze the quiescent model parameters
  - Add additional flaring zone
- Measured variability timescale constrains size of emission region
- Close to SMBH minor changes in the accretion flow could lead to external Compton (EC) emission via inverse Compton (IC) up-scattering of advection dominated accretion flow (ADAF) disc photons
- Naturally explains harder-when-brighter behavior
- Exact acceleration mechanism remains unconstrained

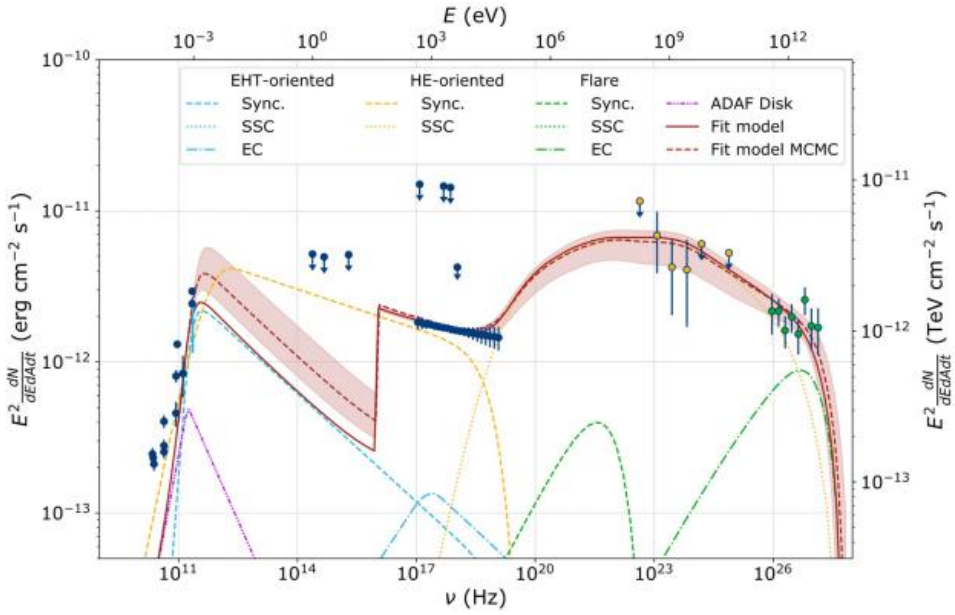

SNR W44

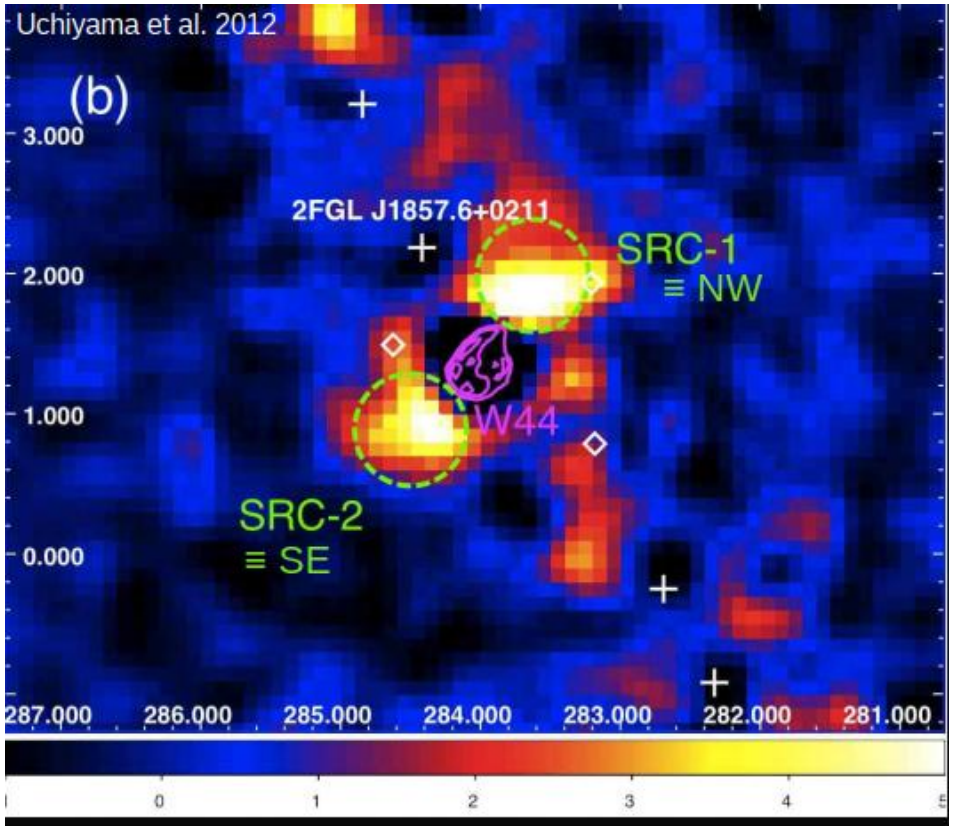

- ~ 10 ky old
- Distance 2.9 kpc ⇒ extended source
- Observed by Fermi-LAT, AGILE

– Low energy cut-off due to pion decay ⇒ known hadronic source

– Two sources found in the vicinity:

SRC-1 ≡ North western (NW)

SRC-2 ≡ South eastern (SE)

– Nearby gas clouds illuminated by escaping cosmic rays?

– Fermi-LAT analysis of ~12 years data

Acceleration and escape of CR from SNR W44

- W44 is a middle-aged SNR embedded in a dense MC.
- GeV gamma-rays detected in NW and SE regions of W44 – can be interpreted as escaping CRs
- Modeled Fermi-LAT + MAGIC observations as the p-p emission of CR escaping from W44 & Galactic CRs on ~ 10^4 Msun MCs

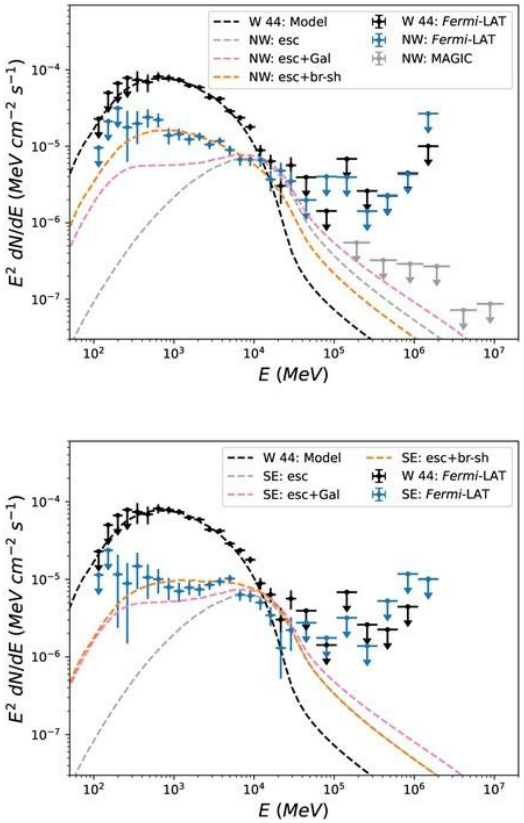

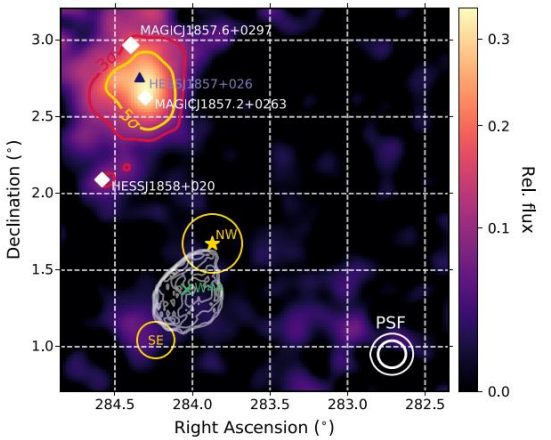

Abe et al. 2025, A&A

W44 by LHAASO - Clear Molecular Clouds and SNR Interaction

LHAASO detect VHE gamma rays extending up to nearly 100 TeV, suggesting the presence of a potential PeVatron.

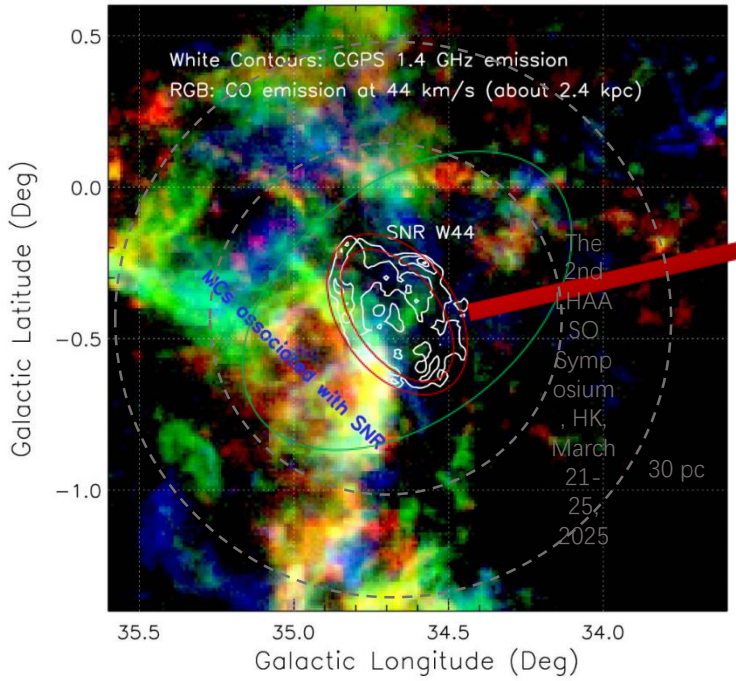

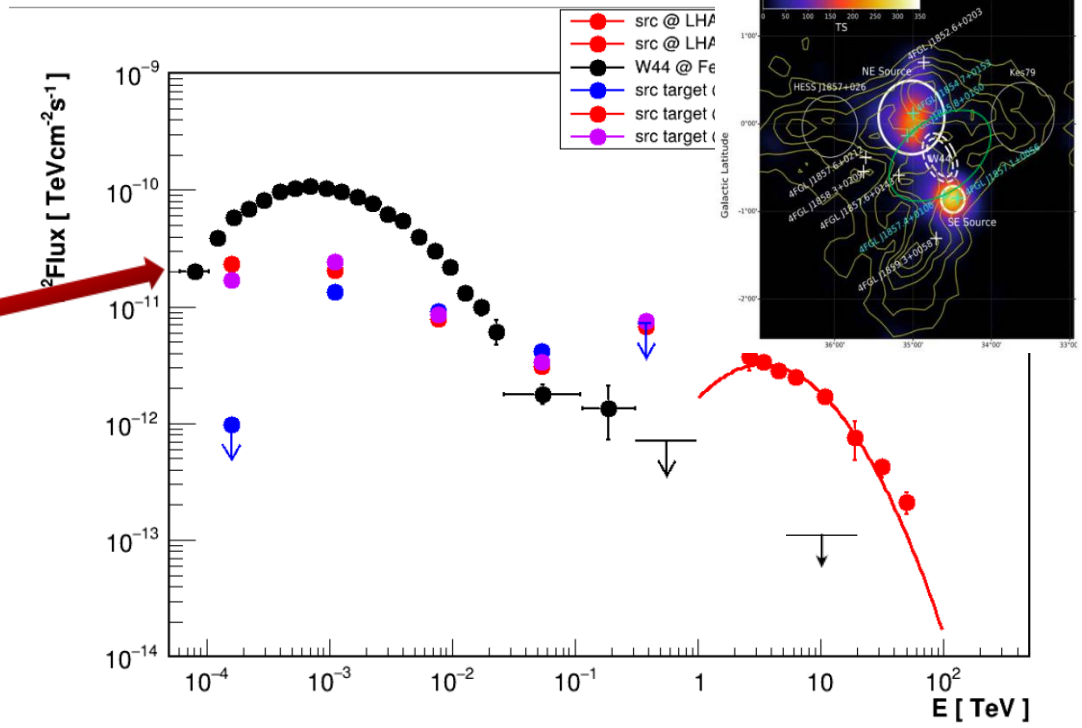

Z. Cao, et al, Symposium of UHE γ-ray from SNR and CR Origin, Yuxi, China, Feb. 2026

1st association of a ~300 TeV neutrino to a γ-ray source

Science 361, July 2018

RESEARCH ARTICLE

NEUTRINO ASTROPHYSICS

Multimessenger observations of a flaring blazar coincident with high-energy neutrino IceCube-170922A

The IceCube Collaboration, *Fermi*-LAT, MAGIC, *AGILE*, ASAS-SN, HAWC, H.E.S.S, *INTEGRAL*, Kanata, Kiso, Kapteyn, Liverpool Telescope, Subaru, *Swift/NuSTAR*, VERITAS, and VLA/17B-403 teams*†

evaluated below, associating neutrino and γ-ray production.

The neutrino alert

IceCube is a neutrino observatory with more than 5000 optical sensors embedded in 1 km^3 of the Antarctic ice-sheet close to the Amundsen-Scott South Pole Station. The detector consists of 86 vertical strings frozen into the ice 125 m apart, each equipped with 60 digital optical modules (DOMs) at depths between 1450 and 2450 m. When a high-energy muon-neutrino interacts with an atomic nucleus in or close to the detector array, a muon is produced moving through

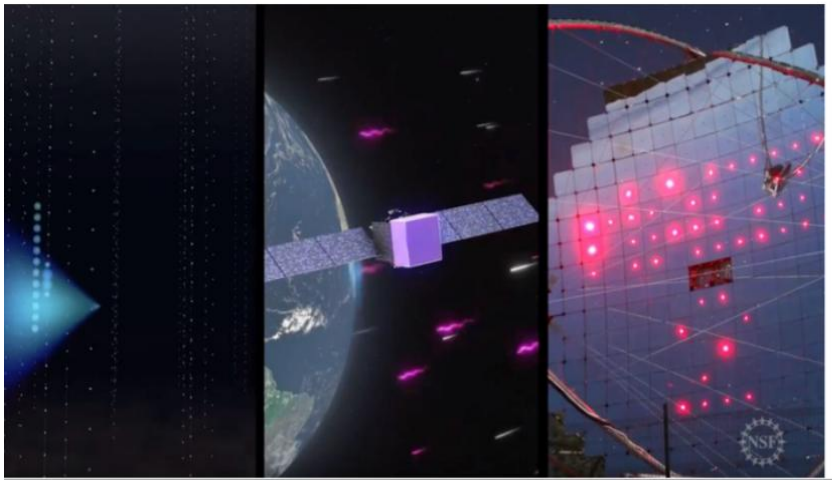

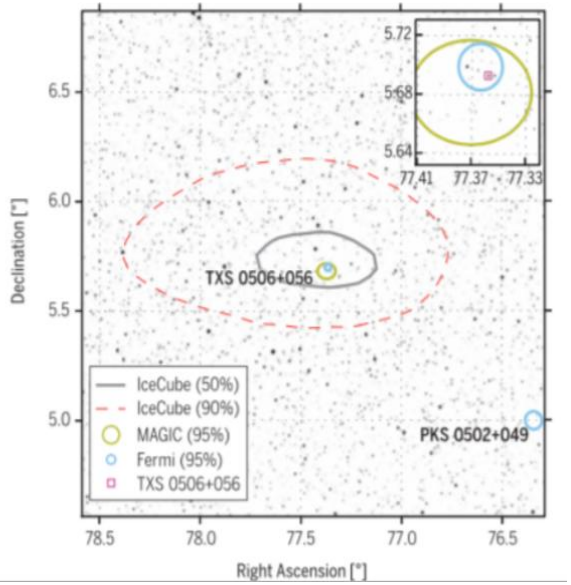

Neutrino – gamma-ray connection

In simple hadronic interaction models ν emission should be comparable to γ's

NGC 1068 – the strongest candidate of TeV ν source - is confronted with an order of magnitude lower limits from MAGIC

MAGIC observations of NGC 4151 (the second-best IceCube candidate) shows similarly strong constraints on the gamma-ray emission

Unlike ν, γ can be easily absorbed

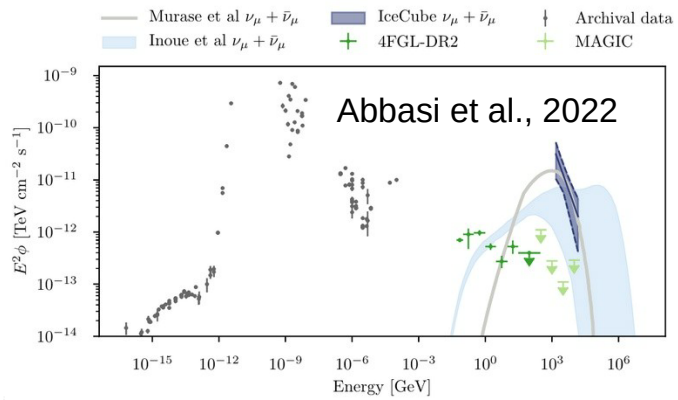

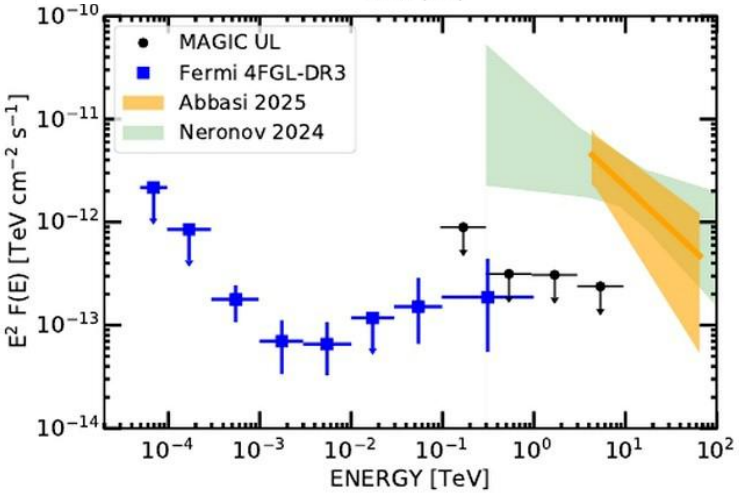

Abe et al. 2025, A&A

LHAASO: Ultrahigh-energy gamma-ray emission associated with black hole–jet systems: SS 433, V4641 Sgr, GRS 1915+105, MAXI J1820+070, Cygnus X-1

National Science Review 12: nwaf496, 2025 https://doi.org/10.1093/nsr/nwaf496

LHAASO study of the source SS 433 is particularly interesting: Its radiation varies with energy. Below 100 TeV, its gamma-ray emission originated from two point-like sources coinciding with the eastern and western lobes of its jet; however, above 100 TeV, the emission becomes an extended source spatially coinciding with a nearby giant atomic cloud identified in past observations by third-party instruments. This part of spectrum could not be fully explained by the Inverse Compton Scattering of electrons (a leptonic process) from the jet itself. Instead, the authors analyzed, it could be associated with the nearby giant atomic cloud: Protons accelerated in the black hole-jet system have diffused out and interacted with the ambient matter in the atomic cloud, producing UHE photons as by-products. In other words, at least part of the UHE gamma rays detected are actually secondary products from protons interacting with the atomic cloud (a hadronic process)

SS433

- SS 433 is a binary system containing a supergiant star that is overflowing its Roche lobe with matter accreting onto a compact object (either a black hole or neutron star).
- Two jets of ionized matter with a bulk velocity of approximately 0.26c extend from the binary, perpendicular to the line of sight, and terminate inside W50, a supernova remnant that is being distorted by the jets.
- SS 433 differs from other microquasars in that the accretion is believed to be super-Eddington, and the luminosity of the system is about 10^{40} ergs per second. The lobes of W50 in which the jets terminate, about 40 parsecs from the central source, are expected to accelerate charged particles, and indeed radio and X-ray emission consistent with electron synchrotron emission in a magnetic field have been observed. At higher energies (≥ 100 GeV), the particle fluxes of γ-rays from X-ray hotspots around SS 433 have been reported as flux upper limits

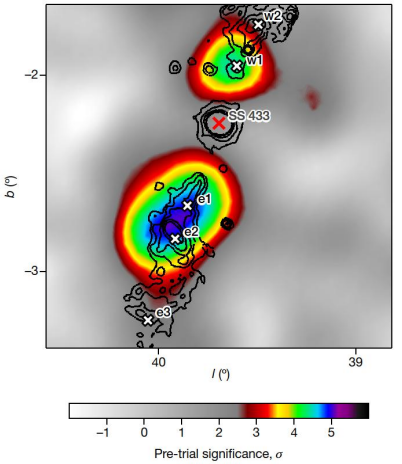

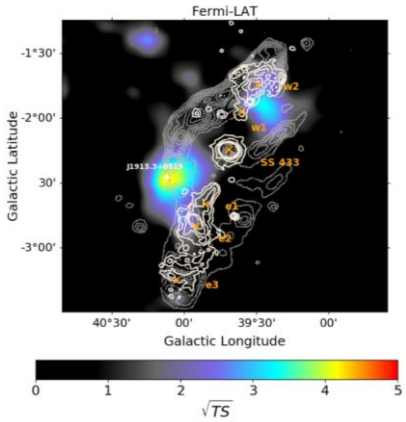

SS433

- In this energy regime, it has been unclear whether the emission is dominated by electrons that are interacting with photons from the cosmic microwave background through inverse-Compton scattering or by protons that are interacting with the ambient gas.
- HAWC reports TeV γ-ray observations of the SS 433/W50 system with spatially resolved lobes. The TeV emission is localized to structures in the lobes, far from the centre of the system where the jets are formed. HAWC have measured photon energies of at least 25 TeV, and these are certainly not Doppler-boosted, because of the viewing geometry. One may conclude that the emission—from radio to *TeV* energies—is consistent with a single population of electrons with energies extending to at least hundreds of TeV in a magnetic field of about 16 μG.

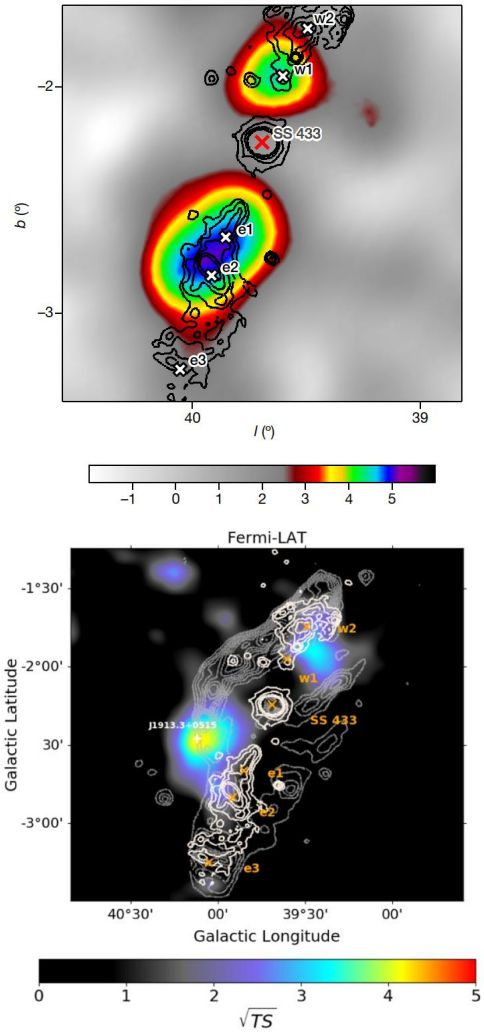

SS433 by HAWC

4 October 2018| Vol. 562 | Nature | 85

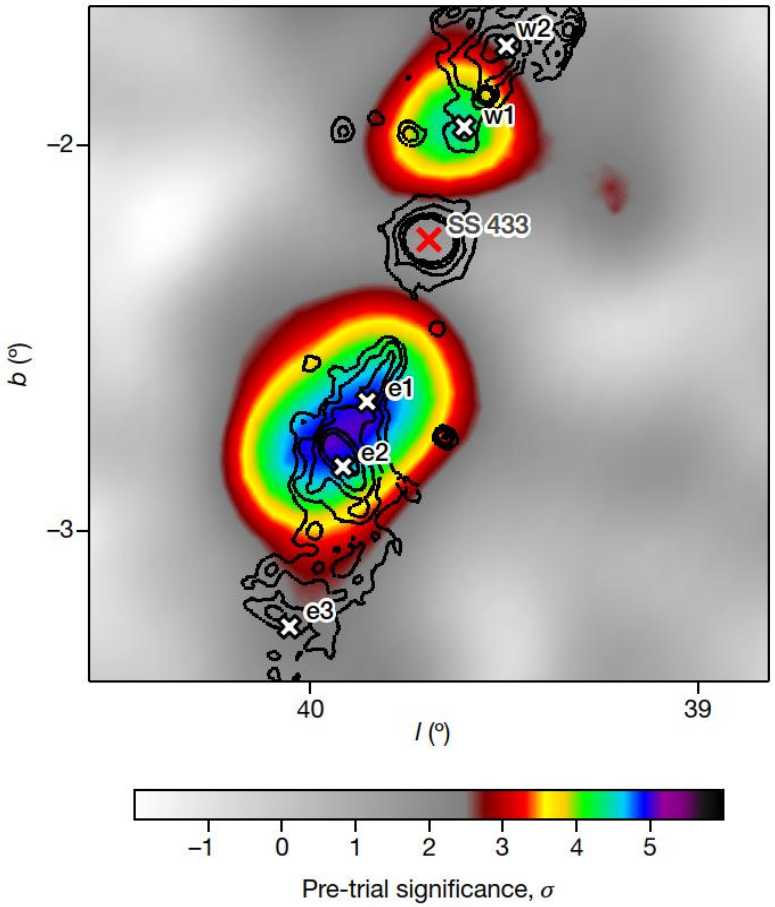

VHE γ-ray image of the SS 433/W50 region in Galactic coordinates. The colour scale indicates the statistical significance of the excess counts above the background of nearly isotropic cosmic rays before accounting for statistical trials. The figure shows the γ-ray excess measured after the fitting and subtraction of γ-rays from the spatially extended source MGRO J1908+06. The jet termination regions e1, e2, e3, w1 and w2 observed in the X-ray data are indicated, as well as the location of the central binary. The solid contours show the X-ray emission observed from this system.

H.E.S.S. Observation of SS433

25 Jan 2024| Vol 383| Science|Issue 6681, 402

Schematic diagram of the model

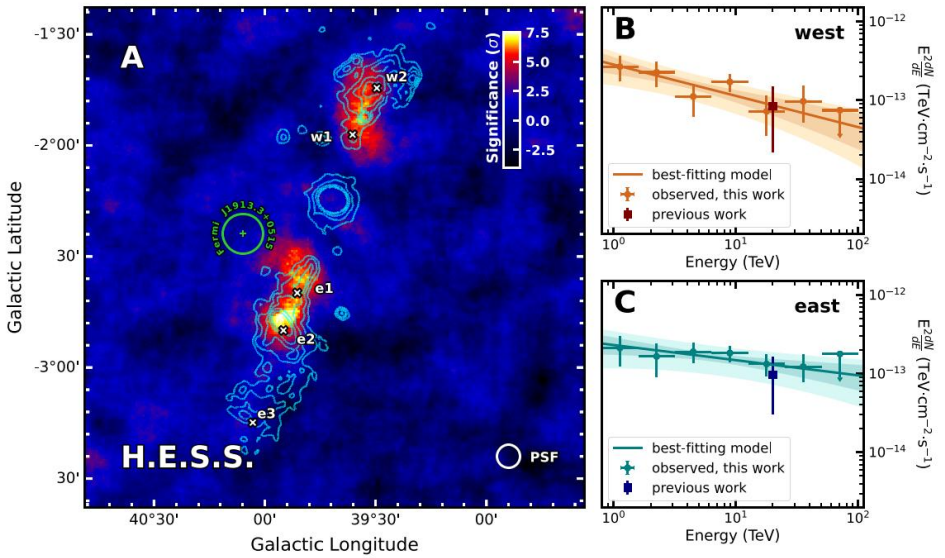

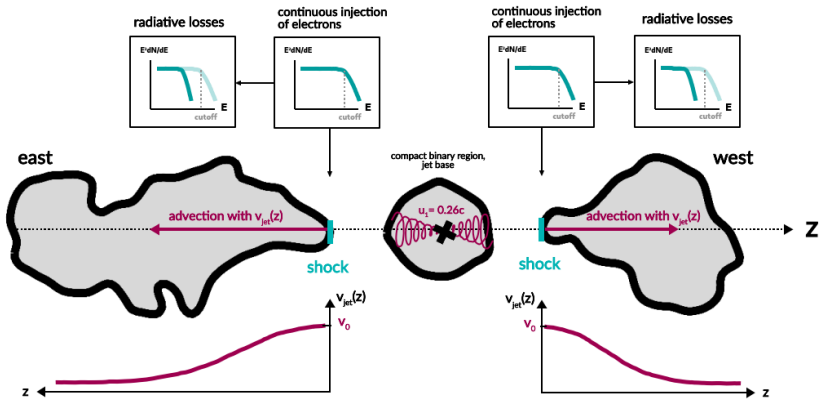

Significance map of the H.E.S.S. observations at energies > 0.8 TeV. Cyan contours show the X-ray emission. White crosses indicate locations of X-ray regions. Significance before accounting for statistical trials and after subtraction of the extended source HESS J1908+063. The green cross indicates the position of Fermi J1913+0515 and the green circle is its uncertainty. B: Orange circular points show our observed spectral energy distribution of the gamma-ray emission from the western jet. C: Same as panel B but for the eastern jet.

SS433, observed by LHAASO

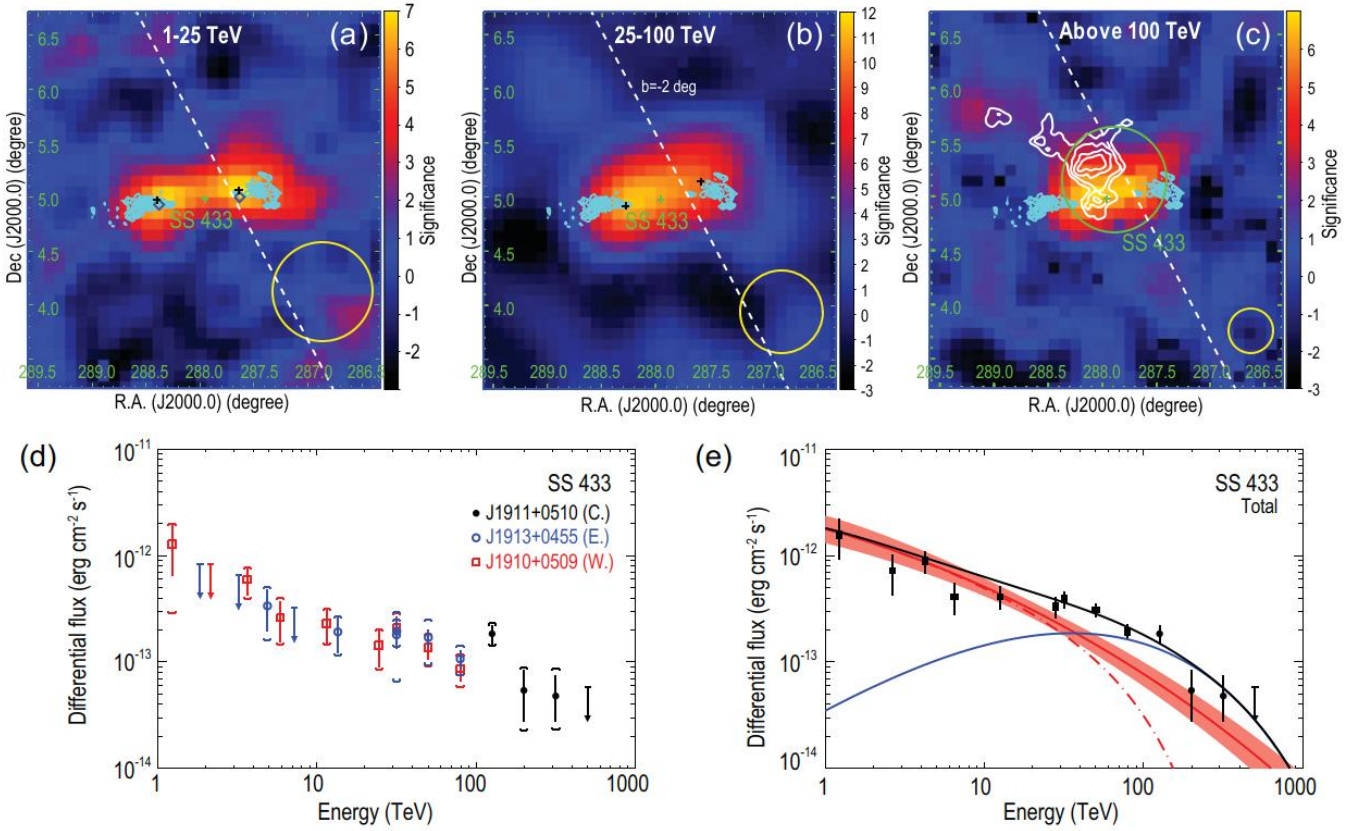

Significance maps and spectral energy distribution of SS 433 measured by LHAASO, with surrounding sources being subtracted. (a–c) SS 433 at energies of 1–25 TeV, 25–100 TeV and above 100 TeV. In the top three panels, the green cross marks the position of the BH of SS 433. In (a), the blue diamonds show the position of H.E.S.S.-detected gamma-ray emission above 10 TeV. In (a) and (b), black crosses indicate the position of two resolved point-like sources at 1–25 TeV and 25–100 TeV.

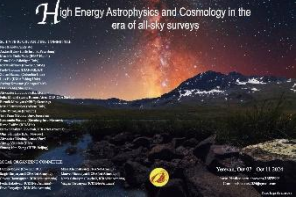

GRB190114C MWL light curves by 2 dozen space & ground-based instruments measured on 14.01.2019

2-papers in *Nature* published by MAGIC in Nov. 2019

- For 1st time GRB measured @ TeV
- Measuring 57 s after onset
- T_{90}~ 360 s, bright, long GRB
- E_{iso}~ 3 x 10^{53} (1keV - 10 MeV)
- Red shift z = 0.4245
- Detected ~ 60σ in afterglow, E ~ 200 GeV – 2 TeV
- TeV and X-ray flux similar
- Intensity > 130 Crab in the first minute
- Purest ever gamma-ray sample

Nature 575, 455-458 (2019) & Nature 575, 459-463 (2019)

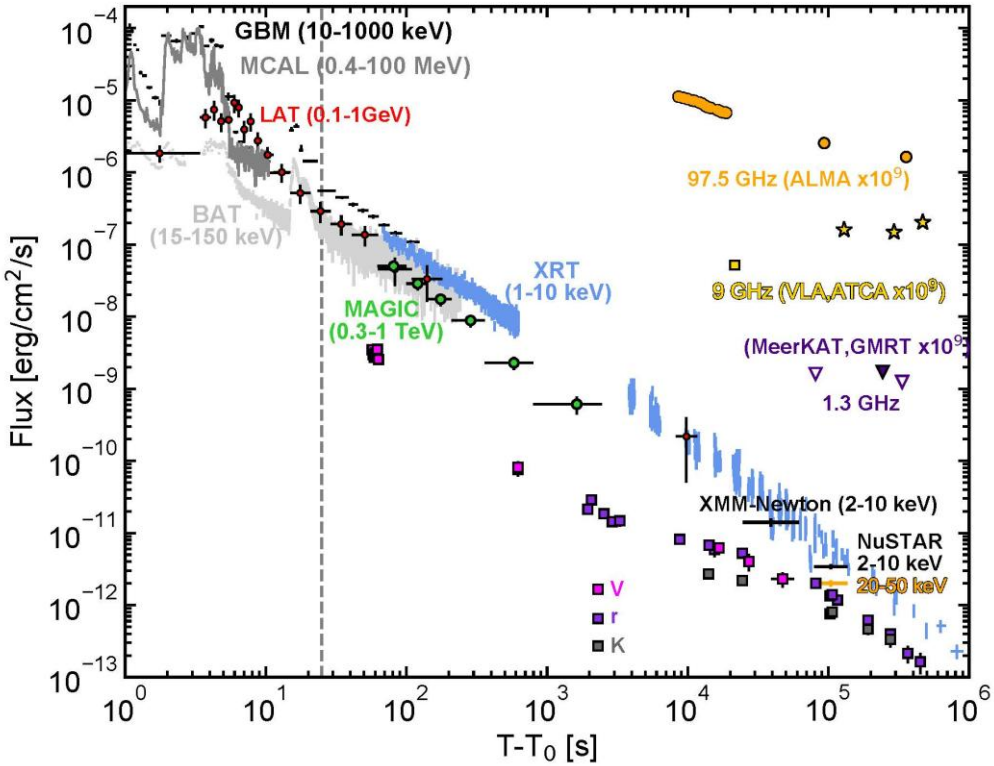

GRBs at TeV

- Currently five GRB-events, all of long type, are detected during the afterglow phase.
- In addition to 1st GRB 190114C, MAGIC detected VHE gamma-rays (70–200 GeV from 56 s to ∼2400 s) from GRB 201216C (Abe et al. 2024), and H.E.S.S. detected VHE emission from GRB 180720B (100–440 GeV at ∼11 h; Abdalla et al. 2019) and GRB 190829A (up to 3.3 TeV; from 4 to 57 h, H.E.S.S. Collaboration 2021).
- In addition, LHAASO detected afterglow radiation up to ∼13 TeV from GRB 221009A (BOAT event) that lasted for 3000 s (LHAASO Collaboration 2023; Cao et al. 2023).

1st GRB 190114C

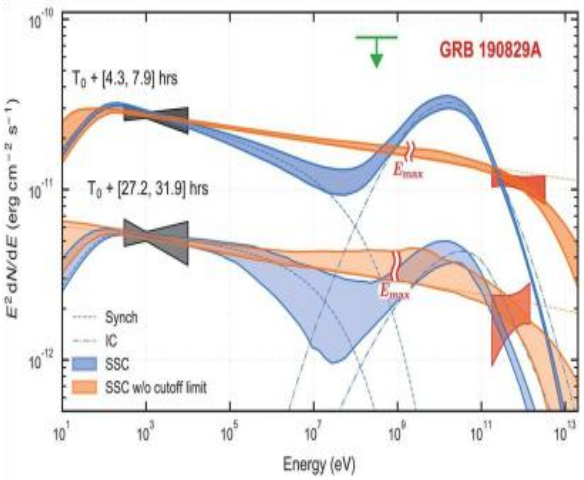

In all these cases, all the VHE data can be successfully described within the SSC scenario (and shows a luminosity similar to that of the synchrotron component.

Appendix A: GRBs observed by MAGIC between 2013 and 2019

Table A.1. List of GRBs observed by MAGIC (under acceptable conditions) between 2013 and 2019.

GRB name	Redshift	Instrument (position)	T_{90} [s]	T_0 [UTC]	T_{start} [UTC]	T_{delay} [s]	Zenith angle [deg]
130502A		*Swift*-BAT	3	17:50:30	20:57:03	11193	33.9-40.1
130504A		*Swift*-BAT	50	02:05:34	02:13:09	455	44.7-56.5
130606A	5.913	*Swift*-BAT	277	21:04:39	21:15:28	649	1.7-46.1
130612A	2.006	*Swift*-BAT	5.6	03:22:22	03:23:08	46	38.0-53.0
130701A	1.155	*Swift*-BAT	4.4	04:17:43	04:18:32	49	15.9-22.6
130903A		INTEGRAL	69	00:47:20	03:57:32	11412	51.9-62.8
131030A	1.295	*Swift*-BAT	41	20:56:19	20:56:45	26	33.7-39.7
140430A	1.60	*Swift*-BAT	174	20:33:36	20:52:06	1110	45.6-73.3
140709A		*Swift*-BAT	98.6	01:13:41	03:22:13	7712	24.6-37.0
140930B		*Swift*-BAT	0.84	19:41:42	21:10:05	5303	18.8-51.4
141026A	3.35	*Swift*-BAT	146	02:36:51	02:38:27	96	16.3-54.1
141220A	1.32	*Swift*-BAT	7.21	06:02:52	06:03:47	55	18.9-24.0
150213A		*Fermi*-GBM	4.1	00:01:48	00:03:08	80	48.2-60.6
150428A		*Swift*-BAT	53.2	01:30:40	01:32:11	91	27.0-57.7
150428B		*Swift*-BAT	131	03:12:03	03:13:03	60	27.0-57.7
150819A		*Swift*-BAT	52.1	00:50:08	02:11:51	4903	37.4-54.4
151118A		*Swift*-BAT	23.4	03:06:30	03:07:14	44	42.8-57.4
151215A	2.59	*Swift*-BAT	17.8	03:01:28	03:01:58	30	15.8-58.0
160119A		*Swift*-BAT	116	03:06:07	03:17:09	662	13.2-58.7
160310A		*Fermi*-LAT	18.2	00:22:57	20:30:16	72439	35.5-40.9
160313A		*Swift*-BAT	42.6	02:37:14	02:39:01	107	30.3-53.3
160504A		*Swift*-BAT	53.9	19:30:36	20:56:29	5153	26.9-33.7
160509A	1.17	*Fermi*-LAT	370	08:59:04	21:21:07 (+2d)	217323	49.2-72.2
160623A	0.367	*Fermi*-LAT	50	05:00:34	02:05:31	75897	27.0-54.7
160625B	1.406	*Fermi*-LAT	460	22:43:24	23:29:38	2774	21.8-54.9
160821B	0.16	*Swift*-BAT	0.48	22:29:13	22:29:37	24	33.4-43.6
160910A		*Fermi*-GBM	24.3	17:19:38	20:21:54	10936	45.4-72.9
160927A		*Swift*-BAT	0.48	18:04:49	20:03:00	7091	32.0-58.8
161229A		*Fermi*-GBM	33.5	21:03:48	23:05:54	7326	22.0-26.1
170728B		*Swift*-BAT	47.7	23:03:19	23:03:58	39	41.8-52.7
170921B		*Fermi*-GBM	39.4	04:02:11	04:48:04	2753	48.4-60.6
171020A	1.87	*Swift*-BAT	41.9	23:07:09	23:08:37	88	13.5-34.9
171210A		*Fermi*-LAT	12	11:49:15	20:33:11	31436	30.9-61.9
180512A		*Swift*-BAT	24.0	22:01:46	22:03:11	85	7.6-38.4
180715A		*Swift*-BAT	0.68	18:07:05	21:27:24	12019	27.9-34.5
180720C		*Swift*-BAT	124.2	22:23:57	22:25:44	107	55.3-55.4
180904A		*Swift*-BAT	5.39	21:28:32	21:30:07	95	23.7-60.2
181225A		*Fermi*-LAT	41.5	11:44:10	19:56:06 (+1d)	115916	46.7-62.6
190106B		*Fermi*-GBM	11.8	20:47:10	20:49:13	123	60.0-60.4
190114C	0.425	*Swift*-BAT	25*	20:57:03	20:58:01	58	55.6-80.0
190829A	0.078	*Swift*-BAT	62.9	19:55:53	02:23:48 (+2d)	109624	37.7-59.6
191004A		*Swift*-BAT	2.44	18:07:02	00:42:30	23728	65.4-69.9

Notes. The GRB redshift, when measured, is reported in the second column. The third column reports the name of the satellite which provided the sky coordinates (e.g. through GCN Notices or Circulars). The forth column reports the prompt emission duration T_{90}. The fifth and sixth columns give the time of the trigger T_0 and the time T_{start} when MAGIC started the observations. The delay T_{delay}(in seconds) is computed as the difference between the start time and the trigger time. The last column reports the zenith angle range related to each GRB observation. *Nominally, the T_{90} of GRB 190114C measured by and GBM is > 300 s. However, most of the emission recorded by and GBM was interpreted as afterglow radiation. The end of the prompt emission can be roughly identified with the end of flux variability, which occurs approximately at 25 s.

Testing the ubiquitous presence of very high energy γ emission in gamma ray bursts with the MAGIC telescopes

Abe, S., et al.: A&A, 700, A96 (2025)

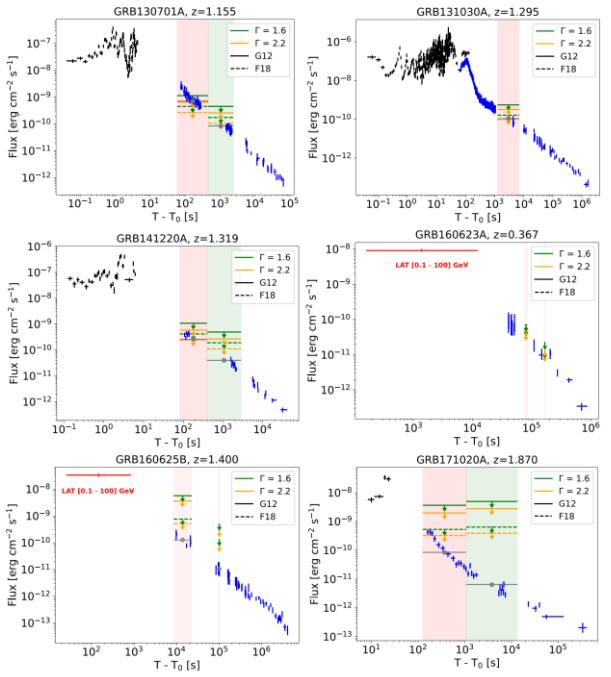

Fig. 4. Multi-wavelength light curves of the subsample of six GRBs described in Sect. 4.2.2 and Table 1. We show the flux light curves with X-ray data (black for BAT and blue for XRT), average X-ray flux in the MAGIC observational time windows (grey points), LAT data (red, if present), and MAGIC ULs assuming two different photon indices and EBL models for the subsample selected for the comparison with lower-energy bands. The time windows in which MAGIC ULs were computed are marked with vertical red and green stripes.

mated the flux ULs at the 95% confidence level following a different approach depending on the available information for the event. For the bursts with an unknown redshift, with a redshift $z \geq 2$, or events that were observed at zenith angle Zd > 40 deg, which are 33 out of 39 GRBs, we computed the night-wise observed flux ULs and we compared these values with the published results of the GRBs detected in the VHE domain and the 2σ level sensitivities of the MAGIC and CTAO-North array at two reference energy values, 150 GeV and 250 GeV. The comparison with the detected GRBs did not reveal any particular difference in terms of their intrinsic properties. The observed ULs are well below the flux points derived from the detected GRBs,

LST-1: early science

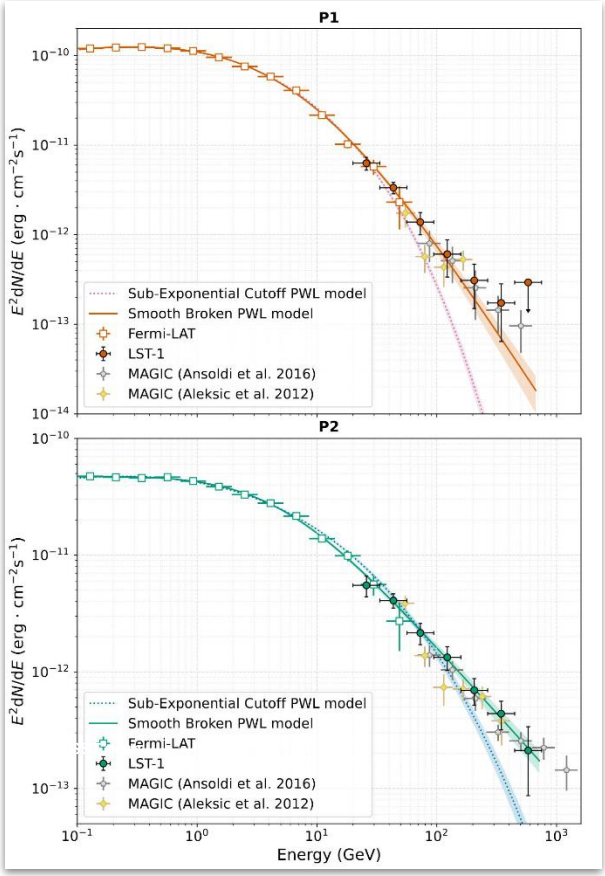

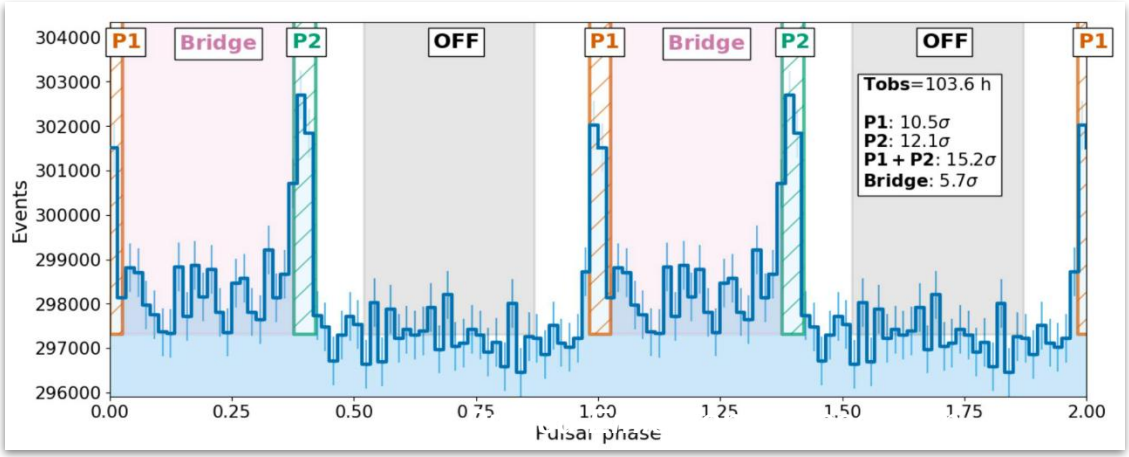

A detailed study of the very-high-energy Crab pulsar emission with the LST-1
A&A, 690, A167 (2024)

Detection of Crab Pulsar:

- Source physics + telescope performances (threshold, cross-calibration, energy resolution…)
- Clear detection of P1 and P2 → **Ethr down to ~20 GeV**
- Smooth transition between *Fermi*-LAT and LST-1

Array Layout

Three zones:

- Inner array:
  - FF=70%, R= 156 m, 2587 tanks
- Outer array:
  - FF= 4%, R= 400 m, 792 tanks
  - FF= 1,7%, R= 560 m, 384 tanks

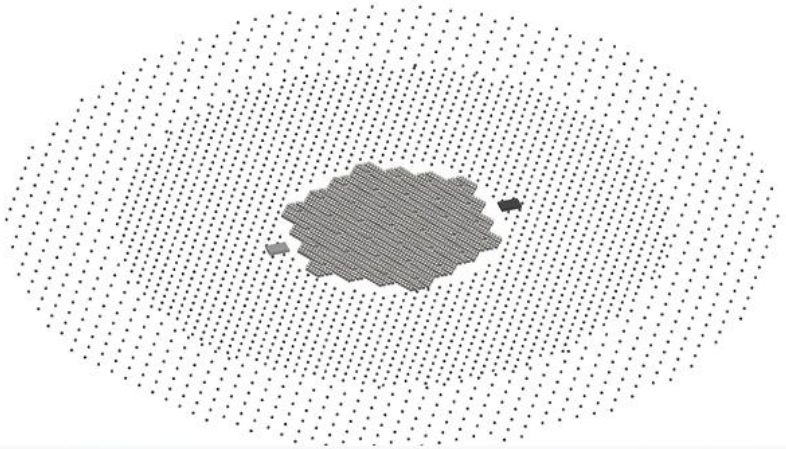

Design of Inner Array

- Steel tanks assembled on site
  - 5.2 m ⌀, 4.1m height
- Double-PMT unit in each detector
  - 10-inch PMTs
- Signals collected at Field Nodes
  - Serve 55 WCDs each

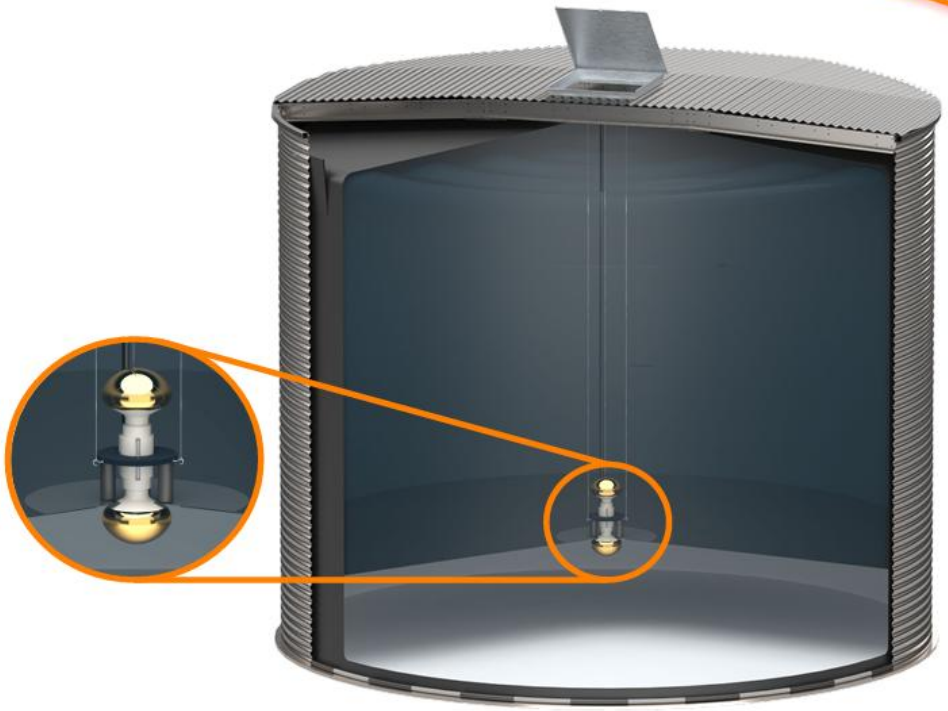

H. Göksu
RICH2025

18

Cherenkov Telescope Array Observatory: CTAO

Two Observation Stations, one Unique Observatory

CTAO

Improved Alpha configuration

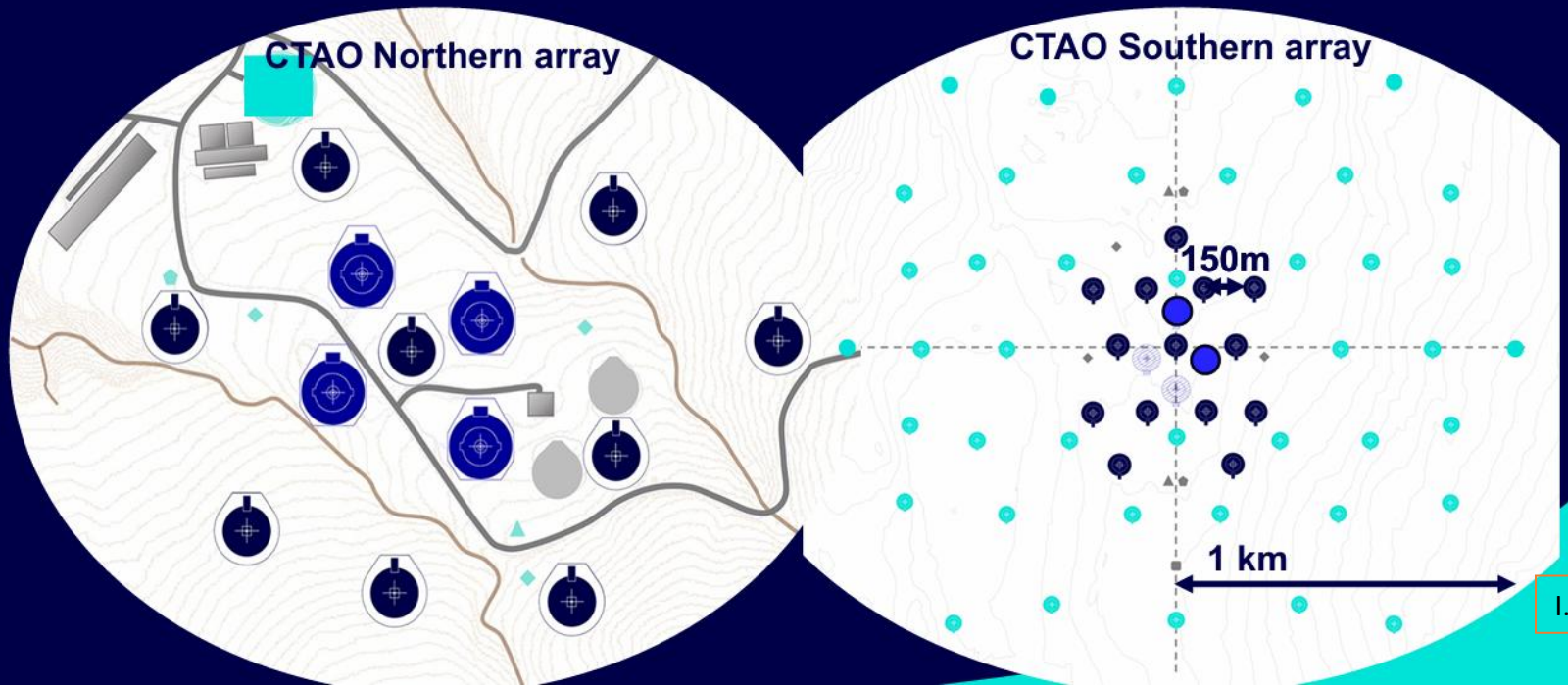

I. Oya, RICH2025

5

SST arrays that are going to strongly impact contemporary astrophysics

LACT: large array of 32 (+4) IACTs of 6m diameter, f/1.33 at LHAASO site, 4400m a.s.l., largest distance ~ 1.3 km

ASTRI mini-array of 9 (+1) telescopes, SCT, double mirror (4.3m & 1.8m) design, on mount Teide on Tenerife on the Canary islands

Plus the array of 37 (+5) SSTs under the construction for the CTAO Southern location in Chile

Telescopes that currently impact astrophysics not only via VHE gamma rays at E ≥ 20 GeV but also via stellar Intensity Interferometry

One can see the two 17m MAGIC IACTs on the left and the 4 CTA/LSTs of 23m ø in the center and right

photo from September 4th

For the time bein we achieved a resolution of ~500 μarcseconds

With the full array there is a potential to o down to ~300 μarcseconds

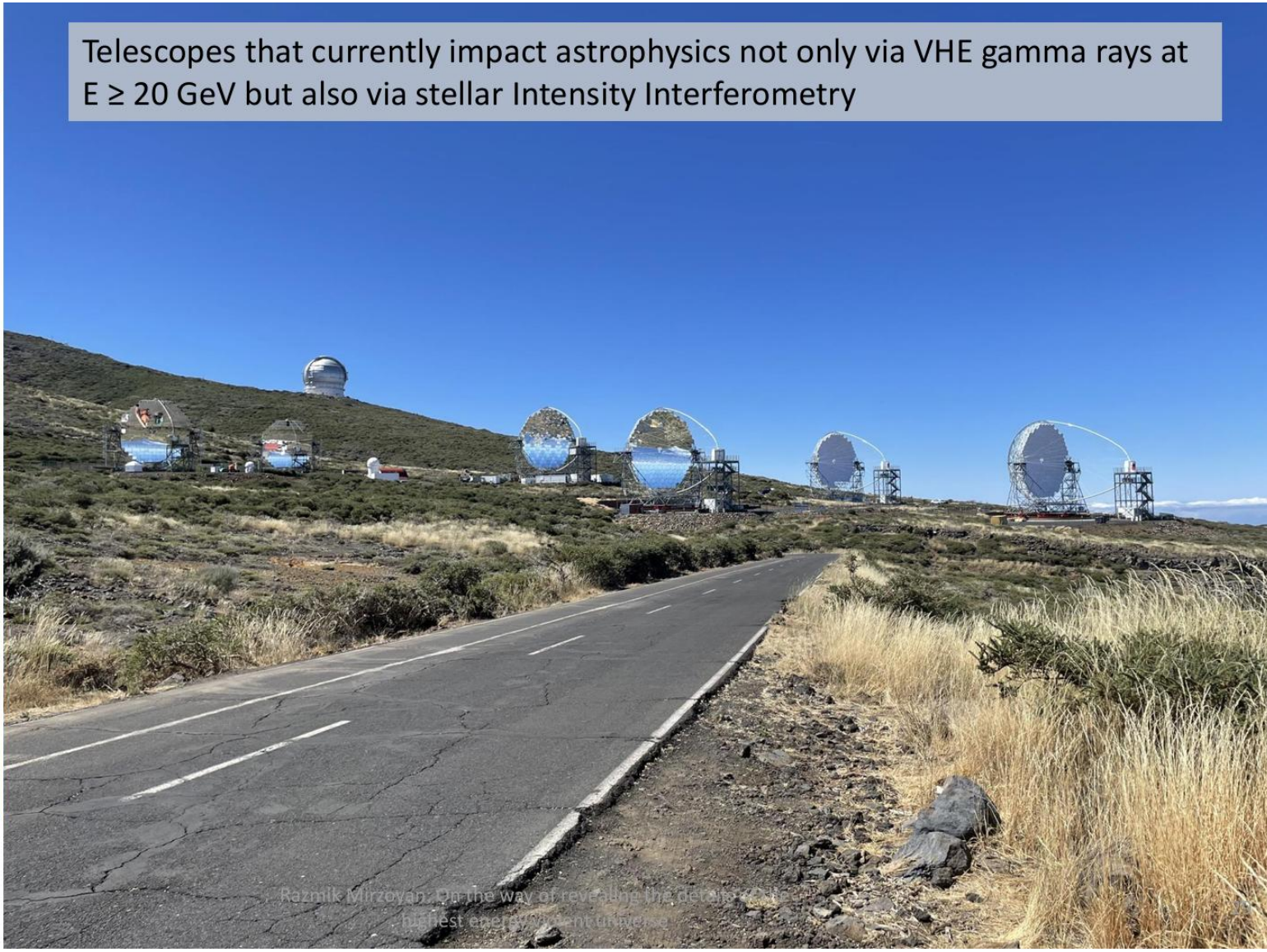

Conclusions

- Gamma-ray astrophysics offers a unique window to explore the most energetic phenomena in the universe.
- The HAWC and LHAASO particle arrays (and, in the future, SWGO) allow us to combine their very high sensitivity (approximately 2,000 hours of observation time per source in the field of view) and excellent background suppression with the 4- to 5-fold higher angular resolution and very high sensitivity of IACT technology (CTAO North and South, ASTRI, and the 32-LACT array in China).
- This combination is of paramount importance for observing the universe in the energy range from 10 GeV to 10 PeV (within six orders of magnitude!).
- These instruments and observatories will be an indispensable component of any multi-wavelength and multi-messenger observation of the universe for the next 20 to 30 years.